Acta Biomaterialia 8 (2012) 61–71

Contents lists available at SciVerse ScienceDirect

Acta Biomaterialia

journal homepage: www.elsevier.com/locate/actabiomat

The effect of processing variables on morphological and mechanical properties of supercritical CO_2 foamed scaffolds for tissue engineering

Lisa J. White [a,*], Victoria Hutter [a], Hongyun Tai [b], Steven M. Howdle [c], Kevin M. Shakesheff [a]

[a] School of Pharmacy, University of Nottingham, Nottingham NG7 2RD, UK
[b] School of Chemistry, Bangor University, Bangor, Gwynedd LL57 2UW, UK
[c] School of Chemistry, University of Nottingham, Nottingham NG7 2RD, UK

ARTICLE INFO

Article history:
Received 8 May 2011
Received in revised form 25 July 2011
Accepted 29 July 2011
Available online 2 August 2011

Keywords:
Supercritical carbon dioxide ($scCO_2$)
Poly(DL-lactic acid) ($P_{DL}LA$)

ABSTRACT

The porous structure of a scaffold determines the ability of bone to regenerate within this environment. In situations where the scaffold is required to provide mechanical function, balance must be achieved between optimizing porosity and maximizing mechanical strength. Supercritical CO_2 foaming can produce open-cell, interconnected structures in a low-temperature, solvent-free process. In this work, we report on foams of varying structural and mechanical properties fabricated from different molecular weights of poly(DL-lactic acid) $P_{DL}LA$ (57, 25 and 15 kDa) and by varying the depressurization rate. Rapid depressurization rates produced scaffolds with homogeneous pore distributions and some closed pores. Decreasing the depressurization rate produced scaffolds with wider pore size distributions and larger, [illegible] 57 kDa $P_{DL}LA$ by $scCO_2$ ensure that these scaffolds are suitable for potential applications in bone tissue engineering.

1. Introduction

The treatment of critically sized bone defects currently involves autograft or allograft transplantation or implantation procedures. The shortage of organ donors coupled with the risk of rejection and disease and the difficulties inherent with artificial implants have led to a great demand for tissue engineered strategies [1,2]. These strategies often use scaffolds, in combination with cells and/or bioactive compounds, to generate new tissue [3]. Considerations for scaffold design are naturally complex and involve not only mechanical and structural constraints but also material composition, degradation properties and products, and surface properties of the scaffold. Additionally, the processing technique must produce scaffolds that can match irregular shapes and sizes of bone defects. The scaffold must promote cell adhesion and growth, and degrade over time into non-toxic components.

Synthetic biodegradable polymers such as poly(lactic acid) (PLA) and poly(lactic acid-co-glycolic acid) (PLGA) copolymers are commonly used in scaffold fabrication as they are approved for certain clinical applications by the US Food and Drug Administration (FDA), degrade in vivo and the degradation products are processed by normal metabolic pathways [4–6]. Scaffolds may be produced from these polymers by a variety of methods, including solvent casting/salt leaching [7–9], phase separation [10,11] and rapid prototyping/solid free-form fabrication [12–15]. These conventional methods, however, generally employ elevated processing temperatures or the use of solvents, which prohibit the incorporation of bioactive molecules in the scaffolds. To overcome these limitations, carbon dioxide (CO_2) has been used as a plasticizer in gas foaming to produce three-dimensional (3-D) polymer constructs [16–20].

CO_2 is a non-toxic, non-flammable, inexpensive reagent that is available in high purity. At a temperature and pressure above its critical point (T_c = 31.1 °C and P_c = 73.8 bar) carbon dioxide is a supercritical fluid, with properties of both gaseous and liquid states [21,22]; the liquid-like density provides much increased solvent power, whilst the gas-like viscosity leads to high rates of diffusion [23]. The addition of supercritical CO_2 ($scCO_2$) to amorphous polymers can produce dramatic changes in the glass transition temperature (T_g), viscosity, interfacial tension and permeability of the polymer [24], and result in the production of foamed materials. Supercritical carbon dioxide ($scCO_2$) foaming is a well-documented process [20,25–33], with two key stages: (i) a soak stage and (ii) a depressurization stage [34]. During the soak, the glassy polymer is saturated with $scCO_2$ at elevated pressures. This acts as a plasticizer, lowering the polymer T_g, and consequently the polymer state becomes rubbery. In the depressurization stage, with temperature constant, the pressure drop from the equilibrium solution state

* Corresponding author. Tel.: +44 1158231232.
E-mail address: lisa.white@nottingham.ac.uk (L.J. White).

1742-7061
doi:10.1016/j.actbio.2011.07.032

induces bubble nucleation; these nuclei grow becoming pores. As the pressure is decreased, the concentration of the plasticizer is also decreased. The polymer T_g increases and vitrification occurs with the porous structure fixed in the glassy state.

Open-cell, interconnected foamed structures are produced by this solvent-free, low-temperature process [35–38]. Drug molecules and proteins can be encapsulated within these constructs as protein structure and activity are retained during processing. Successful applications of this technique include the controlled release of proteins [39,40], promotion of bone formation in vitro and in vivo [41,42] and the induction of angiogenesis in vitro [43].

Scaffold structure is a vital concern in bone tissue engineering. Careful balance must be maintained between optimizing porosity and maximizing mechanical properties in situations where the scaffold may be required to substitute the mechanical function of the tissue that it aims to repair [44]. Whilst highly porous scaffolds (>90%) are needed to ensure cell delivery and tissue ingrowth [45,46], porosities not exceeding 80% are recommended for polymeric scaffolds for implantation into orthopaedic defects [47]. A pore size greater than 100 μm is the minimum recommended for vascularization [48], although more recent in vitro and in vivo studies have suggested that pore sizes and pore interconnections >200 μm may be required [49]. The permeability and interconnectivity of the scaffold are also crucial in determining cell infiltration and successful tissue ingrowth [15].

Recent work on a series of PLGA polymers has shown that modifying polymer composition, molecular weight and foaming process parameters can produce scaffolds with tailored porosities and pore sizes [24]. In this paper, a series of different molecular weights of poly(DL-lactic acid) ($P_{DL}LA$) polymers were employed for a detailed investigation of the effect of the depressurization rate and molecular weight upon scaffold characteristics. This study sought to elucidate the effects of the processing parameters on the porosity, pore size, interconnectivity and mechanical properties of foamed scaffolds as potential devices for bone tissue engineering.

2. Experimental

2.1. Materials

In this study a series of amorphous $P_{DL}LA$ polymers with different inherent viscosity were purchased from Purac (Gorinchem, Netherlands) and Boehringer Ingelheim (Resomer® product) (Ingelheim, Germany), and used as received (Table 1). The weight-average molecular weights (M_w) and polydispersity (*PDI*) of the polymers were determined using gel permeation chromatography (GPC) (PL-120, Polymer Labs) with a refractive index (RI) detector, as described in Ref. [24]. The T_g of the polymers was determined with a TA2920 differential scanning calorimeter. A heating rate of 10 °C min^{-1} was used with a test range of −10 to 120 °C. Food grade CO_2 was supplied by Cryoservice (Worcester, UK) and used without purification.

2.2. Scaffold fabrication

To each well of a Teflon mould was add 130 ± 3 mg of polymer; the mould contained 12 wells, each with a diameter and height of 10 mm (a similar mould is shown in Ref. [35]). The moulds, which were made in-house, had no lid and had a detachable base to facilitate easy removal of scaffolds post-fabrication.

The mould was then placed inside a 60 ml clamp sealed stainless steel high-pressure autoclave (made in-house), which was equipped with a pressure transducer to monitor pressure and a heating jacket with a CAL 3300 temperature controller (CAL Controls, Brighton, UK). HiP (High Pressure Equipment Company, Pennsylvania, USA) high-pressure valves and Swagelok (Ohio, USA) tubing and fittings were used to connect the system. The CO_2 was compressed using a high pressure PM101 pump (New Ways of Analytics, Lörrach, Germany).

The high-pressure vessel was heated to the desired temperature (T) prior to the introduction of CO_2. During the fill time, CO_2 was introduced until the desired pressure (P) was reached. This pressure was maintained during the soak time; the vessel was then depressurized (at a constant rate) to ambient pressure throughout the vent time. The pressure of the vessel in each of the three stages of scaffold fabrication was controlled by a back-pressure regulator (Bronkhorst, Ruurlo, Netherlands) and associated computer software. In this work the desired temperature and pressure were 35 °C and 232 bar, respectively. The porous scaffolds fabricated had diameters of approximately 10 mm and were 5–10 mm in height; a non-porous skin surrounded each scaffold.

2.3. Scaffold characterization

Scaffolds were characterized by micro-X-ray computed tomography (μCT; Skyscan 1174, Skyscan, Aartselaar, Belgium). The μCT was originally designed for non-destructive analysis of unprocessed surgical bone biopsies, but has been adapted for the analysis of polymeric scaffolds [50]. Prior to scanning, the non-porous skin on the scaffolds was removed and scaffolds were cut into uniform cubes, with width, length and height of 5 ± 0.5 mm. The cubic scaffolds were then mounted on a stage at a height of 3 mm within the imaging system and scanned. Measurements were obtained at a voltage of 40 kV, a current of 800 μA and a voxel resolution of 8.9 μm. The transmission images were reconstructed using Skyscan supplied software (NRecon); the resulting 16 bit, 2-D images were saved in tagged image file format (tiff). Quantitative analysis of porosity and pore architecture was obtained using direct morphometry calculations in the Skyscan CTAn software package. The mean pore diameter was calculated by filling maximal spheres into the pores with a distance transformation, as described by Hildebrand and Rüegsegger [51].

In this study, interconnectivity was quantified as the fraction of the pore volume in a scaffold that was accessible from the outside through openings of a certain minimum size; quantitative analysis and a 2-D representation of the process are provided in Ref. [52]. A three-dimensional "shrink wrap" was performed using the Skyscan analysis software to shrink the outside boundary of the volume of interest (VOI) in a scaffold through any openings whose size was equal to or larger than the connection diameter chosen. Connection diameters of 2, 4, 8, 12, 16 and 20 times the voxel size were used in

Table 1
Polymer characteristics.

Polymer	Resource	Form	M_w (kDa)	Inherent viscosity (dl g^{-1})	*PDI*	T_g (°C)
$P_{DL}LA$ (57 kDa)	Purac	Granular	57	0.5	1.87	46.9
$P_{DL}LA$ (25 kDa)	Resomer®	Powder	25.7	0.25–0.35	1.70	47.2
$P_{DL}LA$ (15 kDa)	Resomer®	Powder	15	0.16–0.25	2.34	41.8

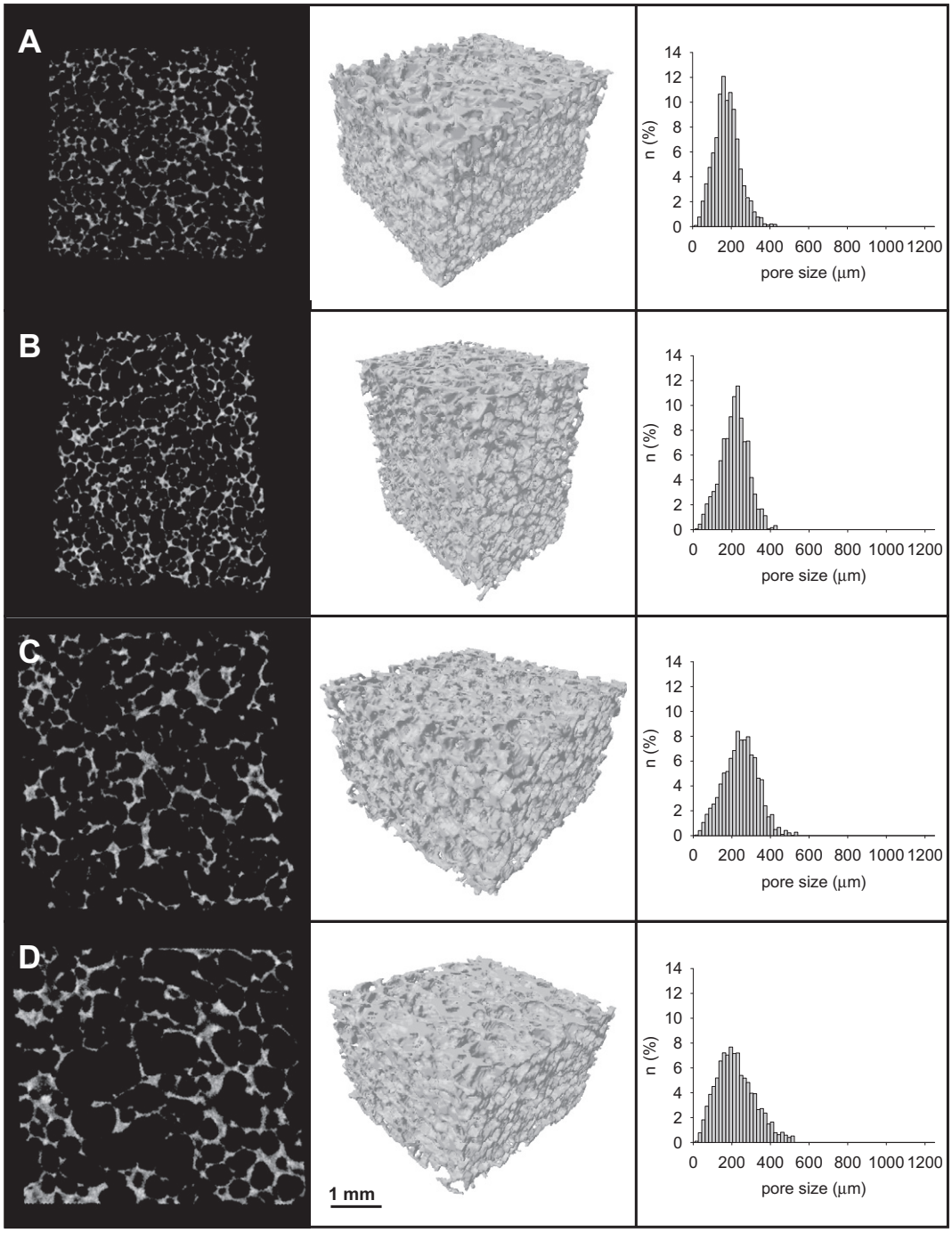

Fig. 1. Effect of depressurization rate on the morphology of $P_{DL}LA$ (M_w = 57 kDa) scaffolds: 2-D slices perpendicular to the direction of foaming (first column), 3-D μCT reconstructions (second column) and pore size distributions (third column). Scaffolds were created with depressurization rates (dP/dt) of (A) 23.2 bar min^{-1}, (B) 7.7 bar min^{-1}, (C) 5.2 bar min^{-1} and (D) 3.9 bar min^{-1}. Scale bar = 1 mm.

this study to give a range of 17–177 μm. Interconnectivity was calculated as follows [53]:

$$\text{Interconnectivity} = \frac{V - V_{\text{shrinkwrap}}}{V - V_s}$$

where V is the total volume of the VOI, $V_{\text{shrinkwrap}}$ is the volume of the VOI after shrink-wrap processing and V_s is the volume of scaffold material.

Compression testing was performed on cubic scaffolds (cut as described above) using the Texture Analyser TA. HD plus (Stable Micro Systems Ltd., Surrey, UK) fitted with a 50 kg load cell. Scaffolds were compressed to a total strain of 60% using a compression speed of 0.01 mm s^{-1}. The compression tests were undertaken at room temperature and applied to the vertically oriented scaffolds, i.e. in the direction of foaming.

The elastic collapse stress (σ^*_{el}), elastic collapse strain (ε^*_{el}) and ultimate stress (σ^*_{ult}) were calculated for each compression test. The slope of the collapse plateau ($\Delta\sigma/\Delta\varepsilon$) was also calculated. The Young's modulus (linear elastic modulus, E^*) was calculated from linear regression on the linear-elastic region of the

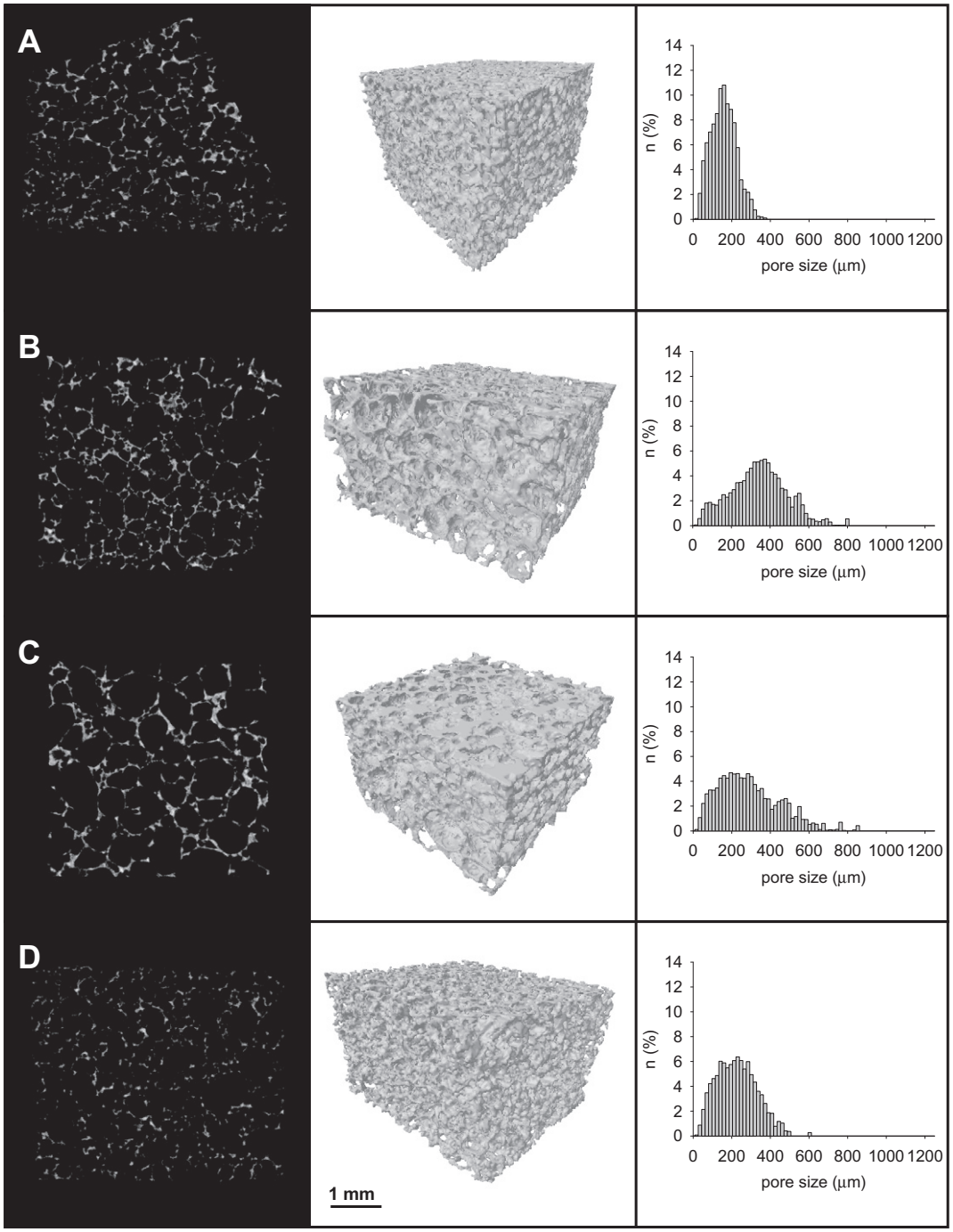

Fig. 2. Effect of depressurization rate on the morphology of $P_{DL}LA$ (M_w = 25 kDa) scaffolds: 2-D slices perpendicular to the direction of foaming (first column), 3-D μCT reconstructions (second column) and pore size distributions (third column). Scaffolds were created with depressurization rates (dP/dt) of (A) 23.2 bar min^{-1}, (B) 7.7 bar min^{-1}, (C) 5.2 bar min^{-1} and (D) 3.9 bar min^{-1}. Scale bar = 1 mm.

stress–strain compression profile. σ^*_{el} and ε^*_{el} were determined from the intersection of E^* and collapse plateau. The compressive strength was the stress produced at 60% strain, i.e. the ultimate stress. The limiting strain of open-cell foamed structures can be calculated if the porosity of the structure is known [54]; an average porosity of 70% (previously observed in foamed scaffolds) was used, which gave rise to the limiting strain of 60% utilized in this work. A minimum of three samples for each foaming condition were analysed and average values (± standard deviation) are reported. Statistical analysis was performed using GraphPad Instat statistical analysis software version 3.06. All values were tested for normality and compared statistically using a Tukey–Kramer multiple comparisons test. Statistical significance between data sets is indicated by $*$ where $p < 0.001$.

3. Results and discussion

$ScCO_2$ foaming of polymers produces 3-D porous scaffolds whose structure (porosity, pore size distribution and interconnectivity) depends upon the process parameters [24,37]. During the soak, the polymer absorbs CO_2 as a function of the temperature, pressure and time, and becomes plasticized. In the depressurization stage, bubble nucleation is induced by supersaturation caused

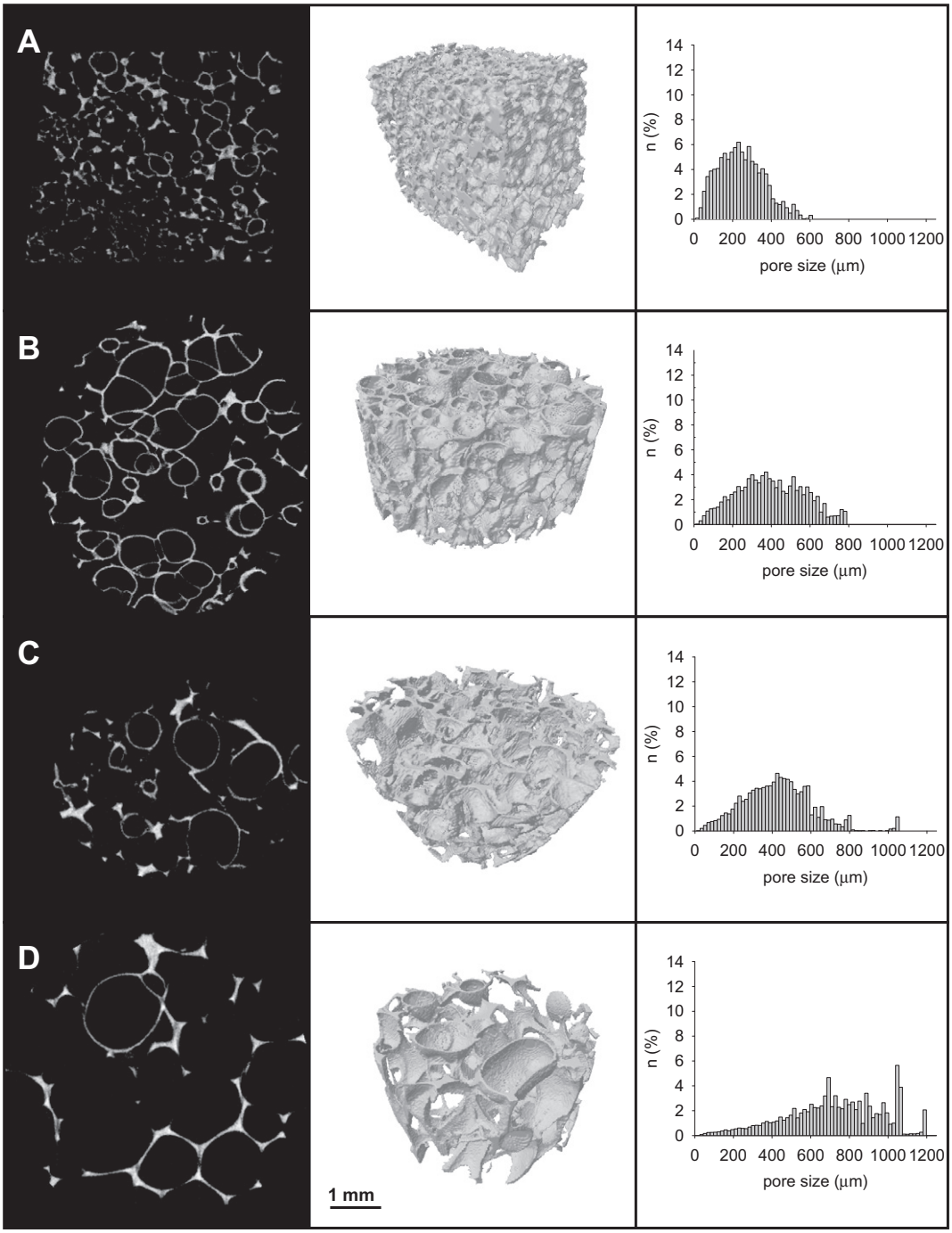

Fig. 3. Effect of depressurization rate on the morphology of $P_{DL}LA$ (M_w = 15 kDa) scaffolds: 2-D slices perpendicular to the direction of foaming (first column), 3-D μCT reconstructions (second column) and pore size distributions (third column). Scaffolds were created with depressurization rates (dP/dt) of (A) 23.2 bar min^{-1}, (B) 7.7 bar min^{-1}, (C) 5.2 bar min^{-1} and (D) 3.9 bar min^{-1}. Scale bar = 1 mm.

by a sudden pressure drop from the equilibrium solution state [23]. The activation energy that must be overcome in order to create stable nuclei depends on the temperature, concentration gradient and pressure gradient [34,55]. In this study, a heating jacket was used to maintain a set temperature during the depressurization stage and nucleation was forced to occur as a result of the pressure drop. The objective of this work was to investigate the effect of depressurization rate (dP/dt) upon the physical morphology and mechanical integrity of scaffolds formed from different molecular weights of $P_{DL}LA$.

The images in Figs. 1–3 show the morphology of the foamed scaffolds at different depressurization rates. $ScCO_2$ foaming of 57 kDa $P_{DL}LA$ produced homogeneous structures with narrow pore size distributions (Fig. 1). The pore size distribution was wider at lower depressurization rates (5.2 and 3.9 bar min^{-1}), as previously observed in foaming of amorphous PLGA [24] and a highly crystalline random co-polymer of ω-pentadecalactone (PDL) and ε-caprolactone (CL) (poly(PDL-CL)) [34]. During the depressurization stage, bubble nucleation is accompanied by and competes with diffusion of gas in the plasticized polymer. This diffusion results in pore

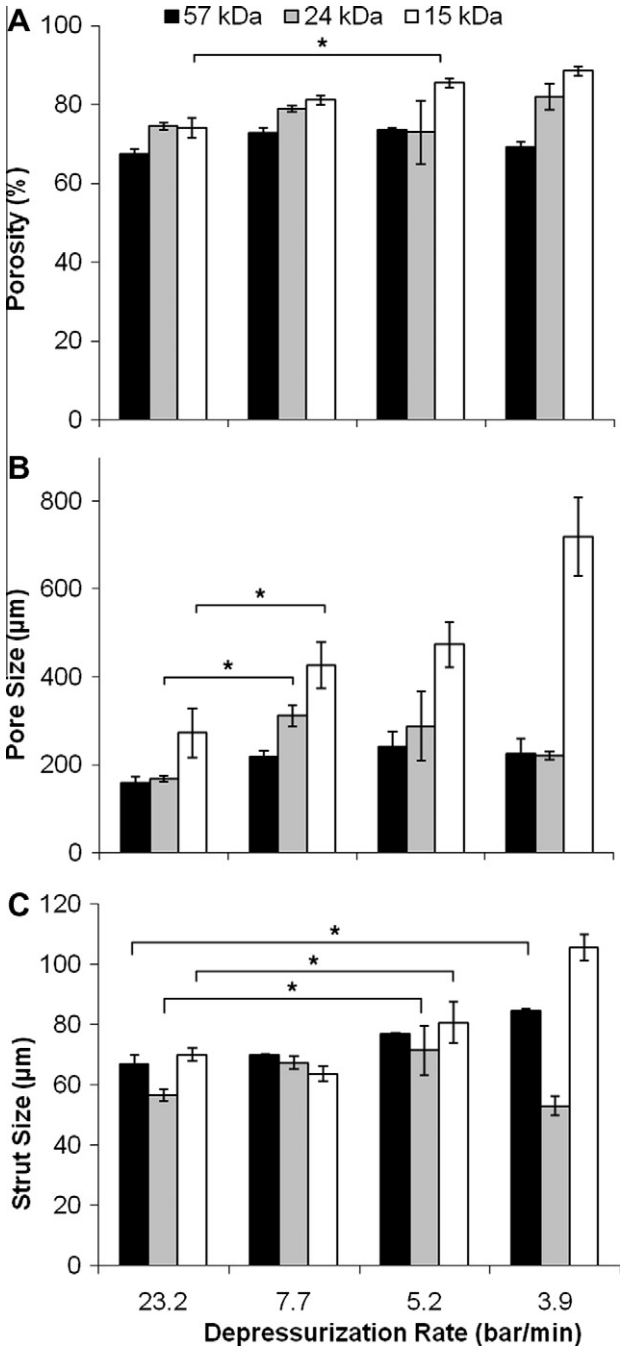

Fig. 4. Effect of depressurization rate on the porosity, pore size and strut size of scaffolds fabricated from 57, 25 and 15 kDa $P_{DL}LA$ with depressurization rates (dP/dt) of 23.2, 7.7, 5.2 and 3.9 bar min^{-1}.

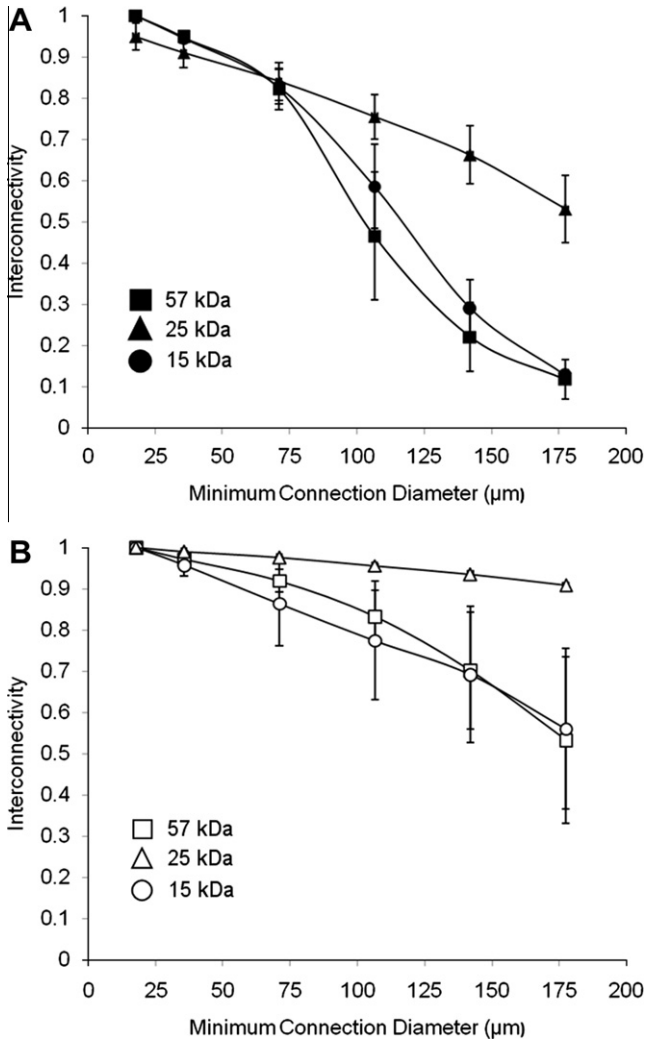

Fig. 5. Interconnected pore space as a function of minimum connection diameter of scaffolds created at depressurization rates (dP/dt) of (A) 23.2 bar min^{-1} and(B)5.2 bar min^{-1}. 57 kDa scaffolds are represented by square symbols, 25 kDa by circular symbols and 15 kDa by triangular symbols, with error bars ($n = 5$) providing mean and standard deviations.

growth. If the depressurization rate is high (fast venting), then nucleation is rapid and a large number of nucleation sites are produced. Diffusion effects are negligible, giving rise to a homogeneous pore size distribution which may contain small closed pores [37]. At lower depressurization rates (slower venting), the pores that are initially nucleated will be significantly larger than others due to greater diffusion opportunities, creating a wider pore size distribution. There is more time for both pore growth and coalescence, generating larger, more connected pores, as can be observed in the comparison of interconnectivity with vent rate, shown in Fig. 5.

No statistically significant differences were observed in the porosities and average pore sizes of the foamed 57 kDa $P_{DL}LA$ scaffolds fabricated with decreased depressurization rates (Fig. 4). An increased strut size was observed between 23.2 and 3.9 bar min^{-1} venting rates. There was no increase in porosity and average pore size between depressurization rates of 5.2 and 3.9 bar min^{-1}, indicating that a plateau had been reached [37].

Scaffolds produced from 25 kDa $P_{DL}LA$ were generally more heterogeneous in structure than those produced from 57 kDa $P_{DL}LA$; wider pore size distributions were achieved at each depressurization rate (Fig. 2), with the exception of 3.9 bar min^{-1}. The pore size distribution was wider at lower depressurization rates, as can be observed at 7.7 and 5.2 bar min^{-1} compared to 23.2 bar min^{-1}. At the depressurization rate of 23.2 bar min^{-1}, rapid nucleation and minimal opportunities for diffusion appear to produce a more homogeneous pore size distribution. As observed in the 57 kDa foams, more connected pores were formed with 25 kDa at lower depressurization rates due to increased opportunities for diffusion, pore growth and coalescence (Fig. 5).

Depressurization rate dramatically affected the structure of scaffolds fabricated with 15 kDa $P_{DL}LA$ (Fig. 3). Akin to 57 and 25 kDa $P_{DL}LA$, the most homogeneous pore size distribution was produced at the highest depressurization rate of 23.2 bar min^{-1}, with many nucleation sites produced during this rapid vent. Decreased depressurization rates (slower vents) produced much

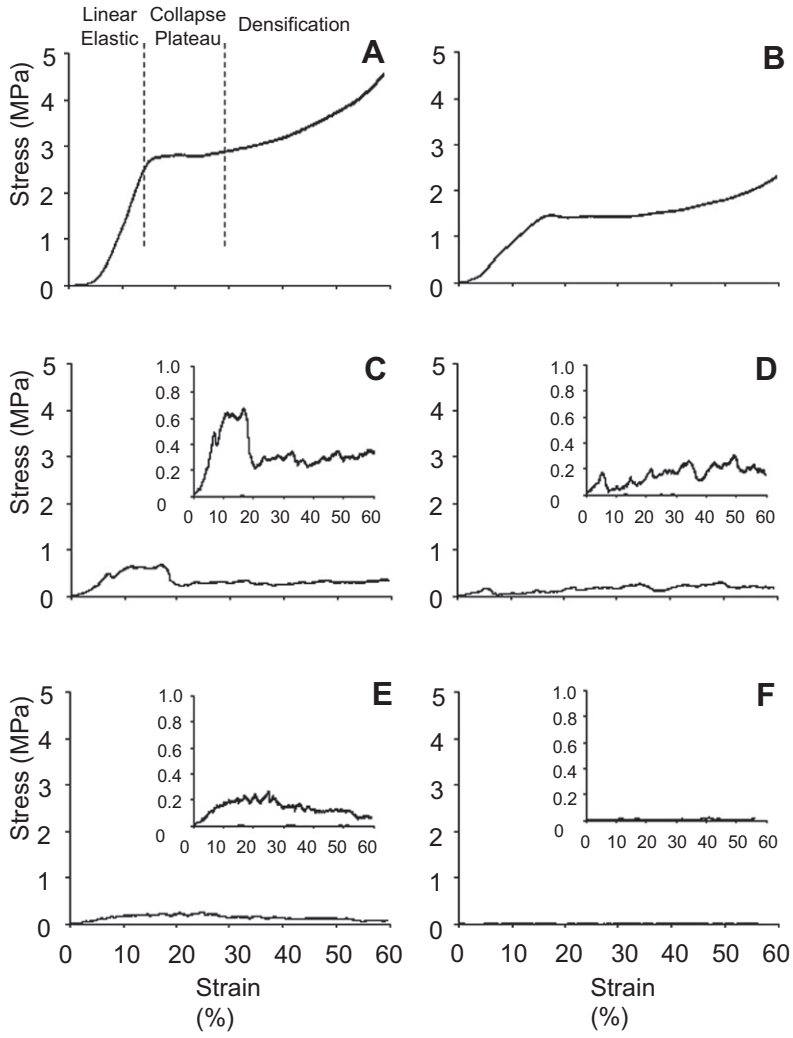

Fig. 6. Characteristic stress–strain curves obtained for foamed scaffolds fabricated from (A, B) 57 kDa, (C, D) 25 kDa and (E, F) 15 kDa $P_{DL}LA$ at depressurization rates (dP/dt) of (A, C, and E) 23.2 bar min^{-1} and (B, D, and F) 5.2 bar min^{-1}. The three distinct regions observed in stress–strain curves for elastomeric open-cell foams are annotated in A.

wider pore size distributions due to diffusion, pore growth and coalescence. The porosity, average pore size and strut size of the foamed 15 kDa $P_{DL}LA$ scaffolds increased with decreased depressurization rate (Fig. 4). It was only possible to cut the scaffold produced at 23.2 bar min^{-1} into the cubic structure used for mechanical testing; scaffolds formed at depressurization rates of 5.2 and 3.9 bar min^{-1} were very fragile, with open structures, as can be seen in Fig. 3(C and D).

The critical parameters for controlling the development of supercritical foamed scaffolds are the concentration of CO_2 in the polymer and the rate of CO_2 escaping from the polymer [56]. These parameters are inextricably linked to the solubility of CO_2 in the polymers, which in turn is dependent upon the morphology and molecular structure of the polymers [24,57]. Thus, the molecular weight and polydispersity (and hence viscosity) of the three polymers studied in this work influence the structure of the foam developed. During the polymer expansion phase, long polymer chains (high molecular weight) may entangle to lock CO_2 in; the short chains (low molecular weight) allow much easier escape of CO_2, which promotes pore growth. This can be seen in Fig. 4, where the pore size of the scaffolds decreased with increased molecular weight; a similar effect was previously observed with PLGA scaffolds [24]. In particular, scaffolds produced from 15 kDa $P_{DL}LA$ (the lowest molecular weight) had much larger pores and fragile structures.

Scaffolds produced at depressurization rates of 23.2 and 5.2 bar min^{-1} were analysed for interconnectivity using the "shrink wrap" plugin in the Skyscan software. Interconnectivity was quantified as the fraction of pore volume of the scaffold that was accessible from the outside through openings of a certain minimum diameter; a range of 17–177 μm was used in this work. Polymer scaffolds fabricated with a faster depressurization rate (Fig. 5A: 23.2 bar min^{-1}) had lower interconnectivity values, in keeping with the homogeneous pore size distributions shown in Figs. 1–3 obtained when diffusion effects are negligible. Closed pores appear to be present in both the 57 and 25 kDa scaffolds; there was a sharp decrease in interconnectivity when the minimum connection diameter was increased above 75 μm. At the lower depressurization rate (Fig. 5B: 5.2 bar min^{-1}) the additional time for growth and coalescence has produced more connected pores for each of the scaffold types. In particular, the high interconnectivity values of the 15 kDa scaffolds reflect the fragile, open structures obtained.

Supercritical processing can produce foams with low interconnectivity [16,20], and in some cases it was been necessary to put salt particles in and leach them out to improve pore interconnectivity [8]. Silica particles have also been used [58] to enhance pore interconnectivity of PLA scaffolds. In this work, the addition of salt or silica was not required as highly connected scaffolds could be achieved by optimizing processing conditions.

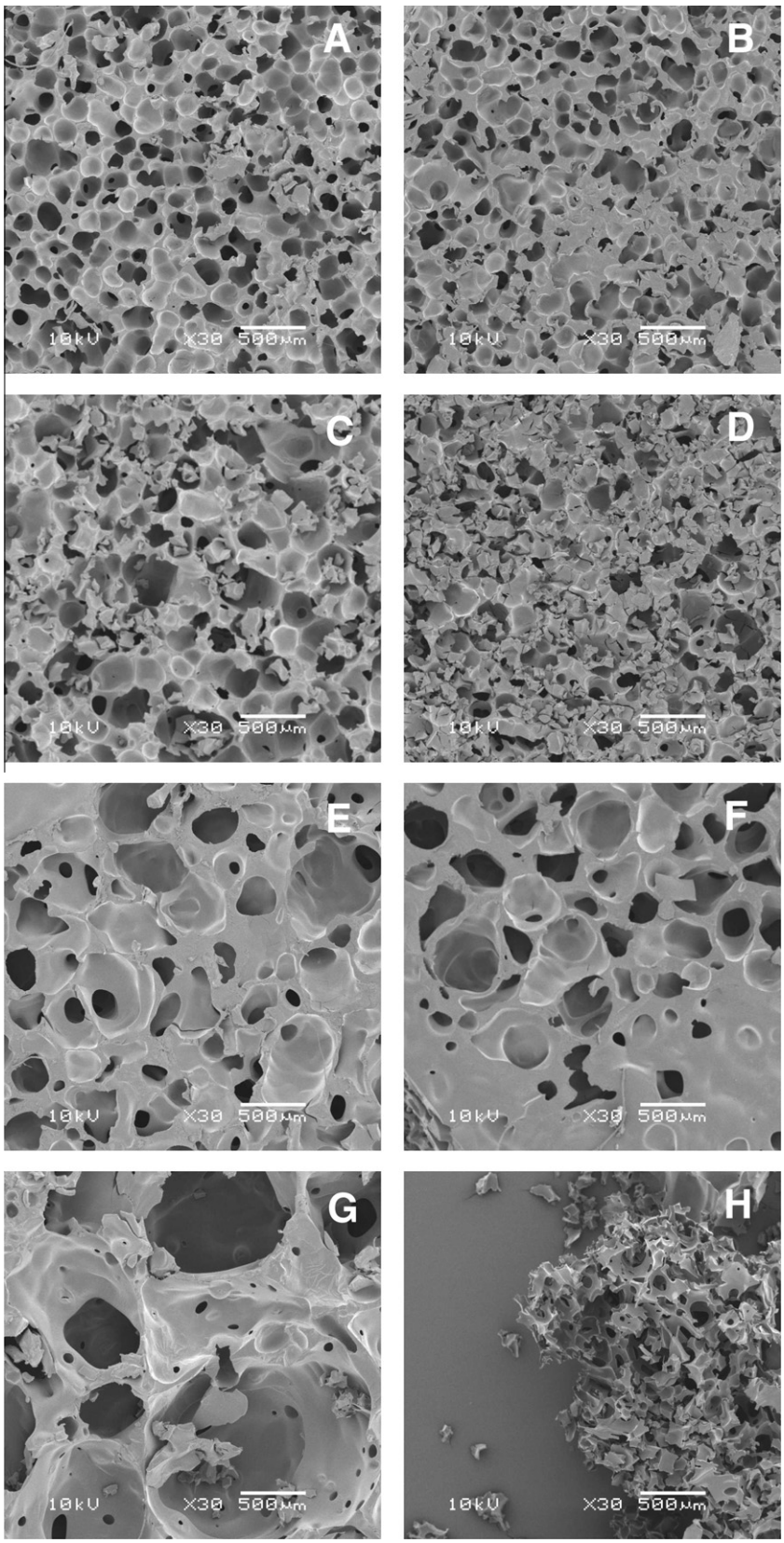

Fig. 7. SEM images of foamed scaffolds before and after compression to 60% strain. Images show the morphology of 57 and 25 kDa scaffolds fabricated with a depressurization rate (dP/dt) of 23.2 bar min^{-1} (A, C) before and (B, D) after compression, and 57 and 25 kDa scaffolds fabricated with a depressurization rate (dP/dt) of 5.2 bar min^{-1} (E, G) before and (F, H) after compression. Magnification 30×; scale bar = 500 µm.

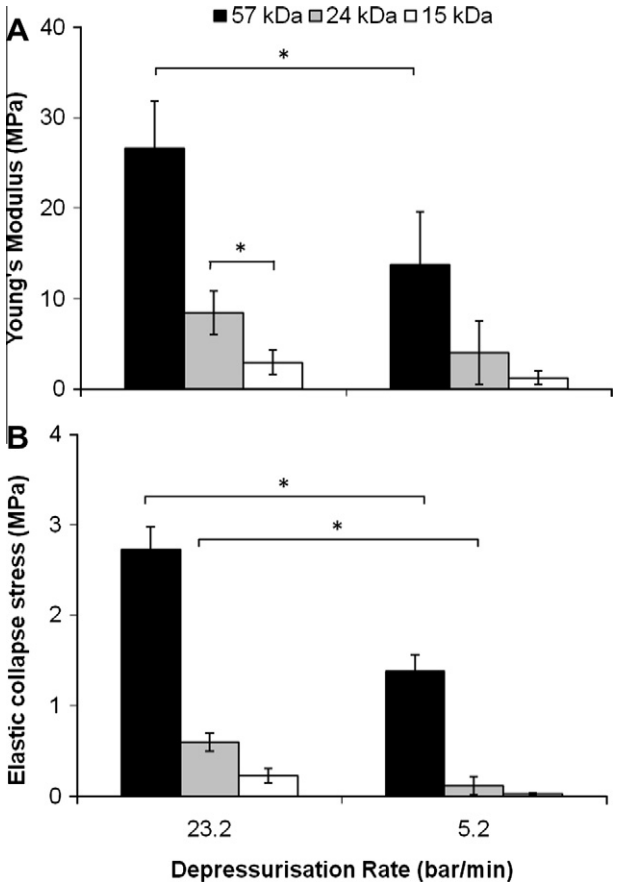

Fig. 8. Effect of depressurization rate on the Young's modulus and elastic collapse stress of scaffolds fabricated from 57, 25 and 15 kDa $P_{DL}LA$ with depressurization rates (dP/dt) of 23.2 and 5.2 bar min^{-1}.

The mechanical properties of foamed structures depend on two sets of parameters: those that describe the geometric structure of the foam and those that describe the intrinsic material properties of the foam. The former set includes the size and shape of foam cells, the way in which material is distributed between cell edges and faces, and the relative density; the latter includes the material density, Young's modulus, plastic yield and fracture strengths. In this work, the mechanical properties of the foamed scaffolds were characterized by compression tests; results are shown for the two depressurization rates (23.2 and 5.2 bar min^{-1}) that produced the most obvious changes in physical morphology.

Thermoplastic polymers such as $P_{DL}LA$ and PLGA can produce foams [54,59] which present different stress–strain curves upon compression. Scaffolds fabricated from 57 kDa $P_{DL}LA$ exhibited typical stress–strain curves for elastomeric open-cell foams (Fig. 6A and B), which are characterized by three distinct regions: a linear elastic regime, a collapse plateau regime and a densification regime [54,60] (annotated in Fig. 6A). The linear elastic regime in elastomeric foams is controlled by cell wall (strut) bending. When loading is compressive, the struts buckle and collapse, giving rise to the collapse plateau, where stress remains relatively constant despite increasing strain. The densification regime results when the cells have almost completely collapsed and opposing walls touch; further strain compresses the solid itself (compaction), giving rise to a final region of increasing stress. Since the integral structure of a foam scaffold is continuous, the structure fails by deformation of the polymer struts surrounding the individual pores.

Open-cell foams collapse at almost constant load, giving rise to a long, flat plateau, as can be observed in Fig. 6B. In closed-cell foams, the compression of gas within the cells, together with membrane stress that appears in the cell faces, give a stress–strain curve which rises with strain [54]. Thus, the stress–strain curve of 57 kDa $P_{DL}LA$ scaffolds fabricated with a depressurization rate of 23.2 bar min^{-1} (Fig. 6A) would indicate the presence of a greater number of closed cells compared to that fabricated with a depressurization rate of 5.2 bar min^{-1} (Fig. 6B). This can also be observed in the interconnectivity values (Fig. 5). The morphology of 57 kDa scaffolds, before and after compression and formed at 23.2 and 5.2 bar min^{-1}, is shown in Fig. 7(A, B, E and F).

The Young's modulus, elastic collapse stress and compressive strength were consistently much higher for the 57 kDa scaffolds than for the 25 and 15 kDa scaffolds (Fig. 8). This trend was also observed with a series of solid cubes manufactured for each polymer molecular weight. The Young's modulus was consistently higher for the 57 kDa cubes, but there was no significant difference between the cubes created from 25 and 15 kDa $P_{DL}LA$ (data not shown). The scaffold morphology and pore structure defined the mechanical integrity for the 57 kDa scaffolds. Increasing the relative density of 57 kDa foams, corresponding to a decrease in porosity in scaffolds fabricated with a depressurization rate of 23.2 bar min^{-1}, led to a statistically significant higher Young's modulus (Fig. 7A). The compressive strength of the 57 kDa scaffolds fabricated at a depressurization rate of 23.2 bar min^{-1} was similar to that described for cancellous (trabecular) bone (2–12 MPa) [61,62]. It has been suggested that low-density trabecular bone resembles an open-cell foam and cellular solids models suggest that trabecular bone fails by elastic buckling [63].

Scaffolds fabricated from 25 and 15 kDa $P_{DL}LA$ did not exhibit the typical stress–strain behaviour of elastomeric open-cell foams, but rather appeared to behave as brittle foams (Fig. 6). This is also apparent in the scanning electron microscopy (SEM) images of the 25 kDa foams, before and after compression and fabricated at depressurization rates of 23.2 and 5.2 bar min^{-1} (Fig. 7C, D, G and H). There was no linear elastic behaviour due to strut bending; instead, a fault line generally propagated through the structure to cause brittle fracture.

Brittle foams collapse by the mechanism of brittle crushing. The crushing strength can be obtained by assuming that strut rupture is constant throughout the structure; the relative density is thus the most important factor affecting mechanical behaviour [64]. However, this was not observed with the 25 and 15 kDa brittle foams. In Fig. 4A the 25 and 15 kDa scaffolds (fabricated at 23.2 bar min^{-1}) possess equivalent relative densities, yet the Young's moduli (Fig. 7A) and compressive strengths (not shown) are significantly different. One possible explanation for this is that the molecular weight of the polymer could dictate the behaviour of the foam. Alternatively, these brittle foams could follow a Weibull distribution [54,64] with an inherent size effect, whereby large specimens fail at lower stresses than small ones because it is more probable that they will contain a larger pre-existing crack. A corollary of this is that, for brittle open-cell foams of the same relative density, the crushing strength decreases with increasing cell size; the strut strength increases with smaller cell sizes. Thus the larger pore size of the 15 kDa foam (Fig. 4B 23.2 bar min^{-1}) dictates that the foam will crush more easily than the 25 kDa foam possessing equivalent relative density but a smaller pore size.

With brittle foams, progressive crushing can lead to a plateau, which ends when the material is completely crushed. The very porous 15 kDa $P_{DL}LA$ foam fabricated at 5.2 bar min^{-1} needed very little strain to crush it (Fig. 6F). The most obvious plateau can be observed in Fig. 6C for the 25 kDa $P_{DL}LA$ scaffold fabricated at 23.2 bar min^{-1}. This structure was the most homogeneous of all the 25 kDa scaffolds. Gibson and Ashby [54] observed that

imperfections in the foam, such as non-uniformities in the relative density (for example, irregular shaped pores or heterogenic pore distributions), can induce cell wall bending. In the case of the brittle foams, although true cell wall bending possibly does not occur, heterogeneity reduces the Young's modulus, most clearly in the case of the 25 kDa foams (Figs. 2A and C and 6C and D).

4. Conclusions

$ScCO_2$ foaming can produce open-cell, interconnected structures in a solvent-free, low-temperature process. Foams of varying structural and mechanical properties can be fabricated from different molecular weights of $P_{DL}LA$ (57, 25 and 15 kDa) and by varying the depressurization rate. Rapid depressurization rates (fast vents) produced scaffolds with homogeneous pore distributions and some closed pores. Decreasing the depressurization rate produced scaffolds with wider pore size distributions and larger, more interconnected pores. In compressive testing, scaffolds produced from 25 and 15 kDa $P_{DL}LA$ behaved as brittle foams and collapsed by the mechanism of brittle crushing. Scaffolds fabricated from 57 kDa $P_{DL}LA$ exhibited typical stress–strain curves for elastomeric open-cell foams. The Young's modulus was increased at high depressurization rates, due to the increased relative density of the foams. Analogous compressive strengths to cancellous bone were achieved with scaffolds fabricated at 23.2 bar min^{-1}. This strength and similarity of mechanical behaviour ensures that 57 kDa $P_{DL}LA$ $scCO_2$ scaffolds are suitable for potential applications in bone tissue engineering.

Acknowledgements

This work was supported by the Engineering and Physical Sciences Research Council, UK, through the "REMEDI" project, Grant No. EP/C534257/1. The authors thank Dr. D.Y.S. Chau, Dr. D. Howard, Dr. G. Kirkham and Dr. L. Hamilton for scientific discussions, and Mr. R. Wilson and Mr. P. Fields for technical assistance.

References

[1] Jones JJ, Hench LL. Biomedical materials for new millennium: perspective on the future. Mater Sci Technol 2001;17:891–900.
[2] Langer R, Vacanti J. Tissue Eng. Science 1993;260:920–6.
[3] Lavik E, Langer R. Tissue engineering: current state and perspectives. Appl Microbiol Biotechnol 2004;65:1–8.
[4] Göpferich A. Mechanisms of polymer degradation and erosion. Biomaterials 1996;17:103–14.
[5] Lu L, Peter SJ, Lyman M, Lai H-L, Leite SM, Tamada JA, et al. In vitro and in vivo degradation of porous poly(-lactic-co-glycolic acid) foams. Biomaterials 2000;21:1837.
[6] Lu L, Peter SJ, Lyman MD, Lai H-L, Leite SM, Tamada J, et al. In vitro degradation of porous poly(-lactic acid) foams. Biomaterials 2000;21:1595.
[7] Ma PX, Choi J-W. Biodegradable polymer scaffolds with well-defined interconnected spherical pore network. Tissue Eng 2001;7:23–33.
[8] Murphy WL, Dennis RG, Kileny JL, Mooney DJ. Salt fusion: an approach to improve pore interconnectivity within tissue engineering scaffolds. Tissue Eng 2002;8:43–52.
[9] Whang K, Thomas CH, Healy KE, Nuber G. A novel method to fabricate bioabsorbable scaffolds. Polymer 1995;36:837.
[10] Chen VJ, Ma PX. Nano-fibrous poly(-lactic acid) scaffolds with interconnected spherical macropores. Biomaterials 2004;25:2065–73.
[11] Chen VJ, Smith LA, Ma PX. Bone regeneration on computer-designed nano-fibrous scaffolds. Biomaterials 2006;27:3973–9.
[12] Hutmacher DW. Scaffolds in tissue engineering bone and cartilage. Biomaterials 2000;21:2529.
[13] Darling AL, Sun W. 3D microtomographic characterization of precision extruded poly-ε-caprolactone scaffolds. J Biomed Mater Res Part B: Appl Biomater 2004;70B:311–7.
[14] Yang SF, Leong KF, Du ZH, Chua CK. The design of scaffolds for use in tissue engineering. Part II. Rapid prototyping techniques. Tissue Eng 2002;8:1–11.
[15] Hollister SJ. Porous scaffold design for tissue engineering. Nat Mater 2005;4:518–24.
[16] Harris LD, Kim B-S, Mooney DJ. Open pore biodegradable matrices formed with gas foaming. J Biomed Mater Res 1998;42:396–402.
[17] Murphy WL, Peters MC, Kohn DH, Mooney DJ. Sustained release of vascular endothelial growth factor from mineralized poly(lactide-co-glycolide) scaffolds for tissue engineering. Biomaterials 2000;21:2521–7.
[18] Sheridan MH, Shea LD, Peters MC, Mooney DJ. Bioadsorbable polymer scaffolds for tissue engineering capable of sustained growth factor delivery. J Control Release 2000;64:91–102.
[19] Richardson TP, Peters MC, Ennett AB, Mooney DJ. Polymeric system for dual growth factor delivery. Nat Biotechnol 2001;19:1029–34.
[20] Mooney DJ, Baldwin DF, Suh NP, Vacanti LP, Langer R. Novel approach to fabricate porous sponges of poly(D,L-lactic-co-glycolic acid) without the use of organic solvents. Biomaterials 1996;17:1417–22.
[21] Cooper A, Howdle S. CO_2 under pressure – a clean solution for polymer processing. Mater World 2000;8:10–2.
[22] Cooper AI. Polymer synthesis and processing using supercritical carbon dioxide. J Mater Chem 2000;10:207–34.
[23] Goel SK, Beckman EJ. Generation of microcellular polymeric foams using supercritical carbon dioxide. I. Effect of pressure and temperature on nucleation. Polym Eng Sci 1994;34:1137–47.
[24] Tai H, Mather M, Howard D, Wang W, White L, Crowe J, et al. Control of pore size and structure of tissue engineering scaffolds produced by supercritical fluid processing. Eur Cells Mater 2007;14:64–77.
[25] Hile DD, Amirpour ML, Akgerman A, Pishko MV. Active growth factor delivery from poly(lactide-co-glycolide) foams prepared in supercritical CO_2. J Control Release 2000;66:177.
[26] López-Periago A, Vega A, Subra P, Argemí A, Saurina J, García-González C, et al. Supercritical CO_2 processing of polymers for the production of materials with applications in tissue engineering and drug delivery. J Mater Sci 2008;43:1939–47.
[27] Mathieu LM, Montjovent MO, Bourban PE, Pioletti DP, Månson JAE. Bioresorbable composites prepared by supercritical fluid foaming. J Biomed Mater Res Part A 2005;75A:89–97.
[28] Mathieu LM, Mueller TL, Bourban P-E, Pioletti DP, Muller R, Manson J-AE. Architecture and properties of anisotropic polymer composite scaffolds for bone tissue engineering. Biomaterials 2006;27:905.
[29] Montjovent MO, Mathieu L, Hinz B, Applegate LL, Bourban PE, Zambelli PY, et al. Biocompatibility of bioresorbable poly(L-lactic acid) composite scaffolds obtained by supercritical gas foaming with human fetal bone cells. Tissue Eng 2005;11:1640–9.
[30] Montjovent M-O, Mathieu L, Schmoekel H, Mark S, Bourban P-E, Zambelli P-Y, et al. Repair of critical size defects in the rat cranium using ceramic-reinforced PLA scaffolds obtained by supercritical gas foaming. J Biomed Mater Res Part A 2007;83A:41–51.
[31] Mandel FS, Popov VK, Howdle SM. Supercritical fluid assisted production of synthetic bone composites. In: Perrut M, editor. 5th Meeting on Supercritical Fluids, International Society for the Advancement of Supercritical Fluids, Nice; 1998. p. 45–50.
[32] Howdle SM, Popov VK. Biofunctional polymers prepared in supercritical fluid. WO9581347 UK; 1998.
[33] Shakesheff KM, Watson M, Whitaker M, Howdle SM. Supercritical fluid assisted production of tissue engineered scaffolds. 7th Meeting on Supercritical Fluids. ISASF: Antibes; 2000. p. 267–72.
[34] Gualandi C, White LJ, Chen L, Gross RA, Shakesheff KM, Howdle SM, et al. Scaffold for tissue engineering fabricated by non-isothermal supercritical carbon dioxide foaming of a highly crystalline polyester. Acta Biomater 2010;6:130–6.
[35] Quirk RA, France RM, Shakesheff KM, Howdle SM. Supercritical fluid technologies and tissue engineering scaffolds. Curr Opin Solid State Mater Sci 2004;8:313–21.
[36] Barry JJA, Howard D, Shakesheff KM, Howdle SM, Alexander MR. Using a core–sheath distribution of surface chemistry through 3D tissue engineering scaffolds to control cell ingress. Adv Mater 2006;18:1406.
[37] Barry JJA, Silva M, Cartmell SH, Guldberg RE, Scotchford CA, Howdle SM. Porous methacrylate tissue engineering scaffolds: using carbon dioxide to control porosity and interconnectivity. J Mater Sci 2006;41:4197–204.
[38] Barry JJA, Silva M, Shakesheff KM, Howdle SM, Alexander MR. Using plasma deposits to promote cell population of the porous interior of 3-D poly(D,L-lactic acid) tissue-engineering scaffolds. Adv Funct Mater 2005;15:1134–40.
[39] Howdle SM, Watson MS, Whitaker MJ, Popov VK, Davies MC, Mandel FS, et al. Supercritical fluid mixing: preparation of thermally sensitive polymer composites containing bioactive materials. Chem Commun 2001:109–10.
[40] Ginty PJ, Barry JJA, White LJ, Howdle SM, Shakesheff KM. Controlling protein release from scaffolds using polymer blends and composites. Eur J Pharm Biopharm 2008;68:82–9.
[41] Yang XB, Whitaker MJ, Sebald W, Clarke N, Howdle SM, Shakesheff KM, et al. Human osteoprogenitor bone formation using encapsulated bone morphogenetic protein 2 in porous polymer scaffolds. Tissue Eng 2004;10:1037–45.
[42] Kanczler JM, Ginty PJ, White L, Clarke NMP, Howdle SM, Shakesheff KM, et al. The effect of the delivery of vascular endothelial growth factor and bone morphogenic protein-2 to osteoprogenitor cell populations on bone formation. Biomaterials 2010;31:1242–50.
[43] Kanczler JM, Barry J, Ginty P, Howdle SM, Shakesheff KM, Oreffo ROC. Supercritical carbon dioxide generated vascular endothelial growth factor encapsulated poly(DL-lactic acid) scaffolds induce angiogenesis in vitro. Biochem Biophys Res Commun 2007;352:135–41.

[44] Hutmacher DW, Schantz JT, Lam CXF, Tan KC, Lim TC. State of the art and future directions of scaffold-based bone engineering from a biomaterials perspective. J Tissue Eng Regen Med 2007;1:245–60.
[45] Freed LE, Vunjak-Novakovic G, Biron RJ, Eagles DB, Lesnoy DC, Barlow SK, et al. Biodegradable polymer scaffolds for tissue engineering. Nat Biotechnol 1994;12:689–93.
[46] Jones JR, Hench LL. Factors affecting the structure and properties of bioactive foam scaffolds for tissue engineering. J Biomed Mater Res Part B: Appl Biomater 2004;68B:36–44.
[47] Goldstein AS, Zhu G, Morris GE, Meszlenyi RK, Mikos AG. Effect of osteoblastic culture conditions on the structure of poly(DL-lactic-co-glycolic acid) foam scaffolds. Tissue Eng 1999;5:421–33.
[48] Freyman TM, Yannas IV, Gibson LJ. Cellular materials as porous scaffolds for tissue engineering. Prog Mater Sci 2001;46:273.
[49] Zhang G, Suggs LJ. Matrices and scaffolds for drug delivery in vascular tissue engineering. Adv Drug Deliv Rev 2007;59:360–73.
[50] Müller R, Matter S, Neuenschwander P, Suter UW, Rüegsegger P. 3D micro tomographic imaging and quantitative morphometry for the nondestructive evaluation of porous biomaterials. In: Briber R, Pfeiffer DG, Han CC, editors. Morphological Control in Multiphase Polymer Mixtures. Mat. Res. Soc. Proc., Cambridge University Press; 1997. p. 217–22. ISSN: 0272-9172.
[51] Hildebrand T, Rüegsegger P. A new method for the model-independent assessment of thickness in 3-D images. J Microsc 1997;185:67–75.
[52] Moore MJ, Jabbari E, Ritman EL, Lu LC, Currier BL, Windebank AJ, et al. Quantitative analysis of interconnectivity of porous biodegradable scaffolds with micro-computed tomography. J Biomed Mater Res Part A 2004;71A:258–67.
[53] Shi X, Sitharaman B, Pham QP, Liang F, Wu K, Edward Billups W, et al. Fabrication of porous ultra-short single-walled carbon nanotube nanocomposite scaffolds for bone tissue engineering. Biomaterials 2007;28:4078–90.
[54] Gibson LJ, Ashby MF. Cellular solids: structure and properties, 2nd ed.. Cambridge: Cambridge University Press; 1997.
[55] Tomasko DL, Li HB, Liu DH, Han XM, Wingert MJ, Lee LJ, et al. A review of CO_2 applications in the processing of polymers. Ind Eng Chem Res 2003;42:6431–56.
[56] Stafford CM, Russell TP, McCarthy TJ. Expansion of polystyrene using supercritical carbon dioxide: effects of molecular weight, polydispersity, and low molecular weight components. Macromolecules 1999;32:7610–6.
[57] Tai H, Upton CE, White LJ, Pini R, Storti G, Mazzotti M, et al. Studies on the interactions of CO_2 with biodegradable poly(DL-lactic acid) and poly(lactic acid-co-glycolic acid) copolymers using high pressure ATR-IR and high pressure rheology. Polymer 2010;51:1425–31.
[58] Collins NJ, Bridson RH, Leeke GA, Grover LM. Particle seeding enhances interconnectivity in polymeric scaffolds foamed using supercritical CO_2. Acta Biomater 2010;6:1055–60.
[59] Lakes R. Materials with structural hierarchy. Nature 1993;361:511–5.
[60] Harley BA, Leung JH, Silva ECCM, Gibson LJ. Mechanical characterization of collagen–glycosaminoglycan scaffolds. Acta Biomater 2007;3:463–74.
[61] Jones JR, Ehrenfried LM, Hench LL. Optimising bioactive glass scaffolds for bone tissue engineering. Biomaterials 2006;27:964–73.
[62] Keaveny TM, Morgan EF, Niebur GL, Yeh OC. Biomechanics of trabecular bone. Annu Rev Biomed Eng 2001;3:307–33.
[63] Gibson LJ. Biomechanics of cellular solids. J Biomech 2005;38:377–99.
[64] Brezny R, Green DJ. The effect of cell size on the mechanical behaviour of cellular materials. Acta Metall Mater 1990;38:2517–26.